Int. J. Electrochem. Sci., 15 **(2020)** 12578 – 12586, doi: 10.20964/2020.12.32

International Journal of
ELECTROCHEMICAL
SCIENCE
www.electrochemsci.org

Short Communication

Phytic Acid Assisted Formation of Phosphorus-Doped Graphene Aerogel as Electrode Material for High-Performance Supercapacitor

Gaosheng Nie[1,*], *Hangchun Deng*[2], *Jie Huang*[2], *Chunyan Wang*[2]

[1] School of Internet of Things, Jiangxi Teachers College, YingTan, Jiangxi, 335000, China
[2] East China University of Technology, Nanchang, Jiangxi, 330013, China
[*]E-mail: n18970187308@163.com

Received: 1 August 2020 / *Accepted:* 30 September 2020 / *Published:* 31 October 2020

In this study, a simple solvothermal method was used to prepare a highly porous phosphorus-doped graphene aerogel (PGA), using graphene oxide (GO) as the precursor and phytic acid as the dopant. The morphostructural characterization of PGA was conducted by scanning electron microscopy (SEM) and X-ray photoelectron spectroscopy (XPS). For supercapacitor applications, PGA materials showed superior capacitance performance (225.3 F g^{-1} at 1A/g) and long-term cycle stability. The specific capacitance retention rate reached 95% after 10,000 charge and discharge cycles. Even if the current density was doubled after 10 times,it can reach 196.8 F g^{-1} (10 A/g). The as-prepared PGA in this study has the advantages of low cost, safety, reliability, and excellent electrochemical performance, and thus has superior application potential.

Keywords: phosphorus-doped graphene aerogel, electrode material, supercapacitors

1. INTRODUCTION

Electrochemical techniques are stable, sensitive, and accurate [1-3], and have been widely used in electrochemical biosensors [4-7], fuel cells [8-10], supercapacitors [11,12], and various other applications. In recent years, with the rapid development of electronic information industry, supercapacitors and other new energy storage devices have attracted much attention [13,14]. Among them, supercapacitors, also known as electrochemical capacitors, fill the big gap between cells and conventional electrolytic or solid capacitors by exhibiting high power density, superior rate capability, rapid charge and discharge rate, long service life, and low maintenance cost [15]. However, supercapacitors still have disadvantages such as low energy density, causing a lag in their applications

[16]. Therefore, an increase in the energy density of capacitors has become a core factor in promoting the development of supercapacitors, and the quality of electrode materials is one of the most key factors that determine the overall performance of capacitors [17].

To supersede commercial activated carbon electrodes, carbon nanomaterials such as xerogel [18], carbon nanotubes [19], porous carbon [20], and graphene [21] have the advantages of high conductivity and large specific surface area (SSA), and they have been widely used in studying EDLC electrodes. Among the existing carbon materials, graphene has received widespread attention because of its ultrahigh dielectric rate and high SSA. Especially supercapacitors based on graphene aerogels have a specific capacitance of 366 F g^{-1} at a current density of 2 A g^{-1} [22]. This high specific capacitance can be attributed to the unique three-dimensional (3D) porous structure, low density, high conductivity, and large SSA [23]. Therefore, it has great potential in diverse sustainable applications such as energy storage, catalysis, and adsorption.

However, graphene is not stable. According to the second law of thermodynamics, graphene will reduce its own energy through spontaneous agglomeration and make itself more stable [24]. Therefore, in practical applications, the SSA and electrical conductivity of graphene are much smaller than theoretical values. To solve these problems, graphene can be doped. The introduction of dopant atoms not only helps to introduce structural defects, but also changes the electron distribution in the graphene layer. This reduces the energy of graphene, provides a location for specific adsorption, and probably generates redox-active surface entities, thereby effectively eliminating agglomeration, providing the advantages of its high SSA, and enhancing the capacitance of the electrode [25, 26]. At present, graphene doping has been extensively studied, such as doping with N [27], S [28, 29], B [30], and F [31] atoms. P and N have the same number of valence electrons, and a larger radius of P atom relative to the radius of C atom will cause the structural deformation of hexagonal carbon skeleton. The length of P-C bond is longer than the length of C-C bond, making P protrudes from the graphene plane. This can lead to an increased surface area and increased separation of graphene layers [32].

Herein, we report a convenient and effective method to prepare P-atom doped graphene sheets with a porous structure. Using graphene oxide (GO) as a precursor and phytic acid as a dopant, P-doped graphene aerogel (PGA) was prepared using a simple solvothermal method. C-P bond not only provides enough electrochemical defects for PGA electrode, but also ensures a high conductivity of PGA. The results show that the prepared PGA electrode has significant specific capacitance, excellent rate performance, and long-term cycle stability.

2. EXPERIMENTAL

2.1. Chemicals

Phytic acid, ethylene glycol, potassium permanganate ($KMnO_4$), potassium hydroxide (KOH), sodium nitrate ($NaNO_3$), 98% sulfuric acid (H_2SO_4), and 30% hydrogen peroxide (H_2O_2) were obtained from China Medicine Co. Natural graphite powder was purchased from Nanjing Xianfeng Co., and the solutions were prepared with redistilled water obtained from a pure system (>18 MΩ).

2.2. Preparation of PGA

GO was prepared using a modified Hummer’s method [33,34] using natural graphite powder as the starting material. PGA was prepared using a simple solvothermal method. 0.1 g GO powder and 1 g phytic acid were dispersed in 200 mL ethylene glycol and sonicated for 3 h. Next, the mixture was transferred into a 500 mL dried autoclave. The reaction was kept at 150 °C overnight. After cooling to 20-30 °C, the samples were separated by centrifugation, washed with distilled water and ethanol for 3-5 times, and then freeze-dried for 36 h. Finally, the samples were heated at 700 °C for 3 h under argon flow. For comparison, undoped graphene aerogels (UGA) were prepared through the same process except the addition of phytic acid.

2.3. Electrochemical Characterization

Electrochemical measurements were carried out using a CHI660E electrochemical workstation equipped with a three-electrode system in 6 M KOH aqueous electrolyte solution. A saturated calomel electrode (SCE) and Pt wire served the reference and counter electrode, respectively. The working electrode was prepared by mixing PGA (85 wt%), with PTFE (5 wt%) and carbon black (CB, 10 wt%) and then pressed onto a Ni foam (1 cm × 2 cm) and dried under vacuum. Cyclic voltammetry (CV) and galvanostatic charging/discharging (GCD) techniques were used to evaluate the electrochemical performance of PGA electrode. Specific capacitance was calculated from the galvanostatic charge/discharge curves using the following equation

$$\mathrm{C}=\frac{I\cdot t}{m\cdot\Delta U}$$

where I is the discharge current, t is the discharge time, m is the mass of active material, and ΔU is the voltage window (here, $\Delta U = 1$ V).

2.4. Characterization of materials

SEM image was obtained using a JEM-2100F transmission electron microscope. XPS analyses were performed using a Thermo Fisher X-ray photoelectron spectrometer equipped with Al radiation as the probe (Kα radiation) with a chamber pressure of 5×10^{-9} Torr. The analysis spot size was 400 μm in diameter.

3. RESULTS AND DISCUSSION

3.1. Form and structure of PGA

Figure 1 shows the SEM image of PGA material. The material has a thin layer and folded structure with typical graphene characteristics. This indicates that the experiment successfully afforded a graphene electrode material with a 3D structure using hydrothermal method. The 3D structure of

PGA material allows a certain space between graphene sheets, conducive to the infiltration of electrolyte and diffusion of electrolyte ions inside the electrode. This can effectively inhibit the agglomeration effect of graphene nanometer sheets and improve the effective SSA of graphene materials. Moreover, owing to the electronegativity and different bond angles doped by heteroatoms (P), defects are caused in the graphene lattice and folds on the surface of PGA film.

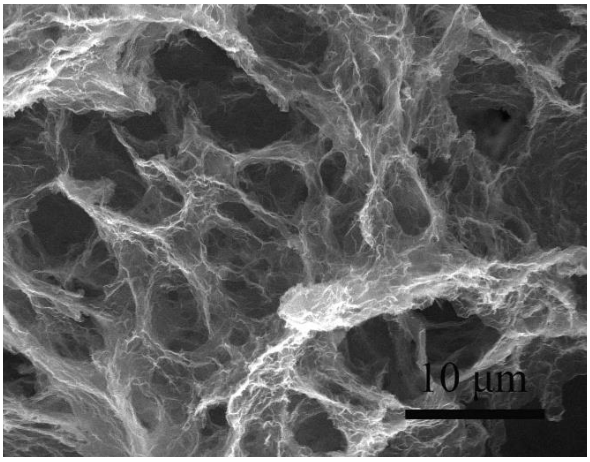

Figure 1. SEM image of PGA

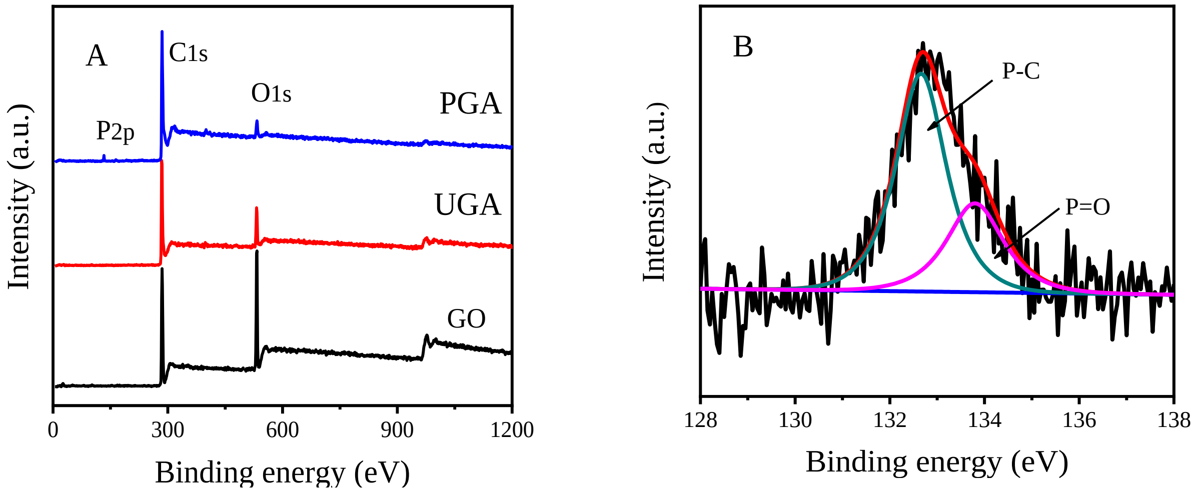

Figure 2. (A) XPS spectroscopy of GO, UGA, and PGA; high-resolution XPS P2p spectra of PGA

XPS was used to study the elemental composition and chemical state of PGA. Figure 2A shows the full XPS spectrum of GO, UGA, and PGA. As shown in Figure 2A, the peaks at 132, 285, and 534.0 eV correspond to P, C, and O, respectively. The wide-range XPS spectrum of PGA clearly shows another small peak P2p compared with GO and UGA. This represents the successful chemical doping of P atoms on graphene sheet frames. In addition, the O 1s peak of PGA and UGA samples is much smaller than the O 1s peak of GO, indicating that GO-containing functional groups with a higher oxygen content are partially eliminated or even disappeared during the hydrothermal process.

The high-resolution P2p spectrum of PGA is shown in Figure 2B; the two peaks at 132.6 eV and 133.8 eV correspond to the C-P bond and P=O bond, respectively. Therefore, we speculate that the C-P covalent bond is formed by the condensation reaction of GO and phytic acid [35]. Most of the C-P=O bonding exists on the surface of reduced GO, as confirmed by previous studies [36]. All these XPS analyses strongly prove that P was successfully incorporated into the layered graphene structure to form a covalent C-P bond.

3.2. Electrochemical Performance

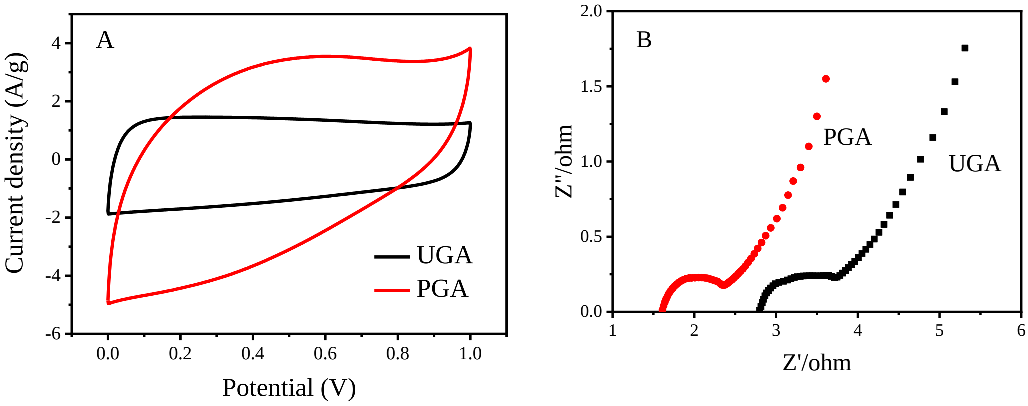

Figure 3. (A) CV curves of UGA and FGA in 0.5 M Na_2SO_4 solution at 20 mV/s, (B) Nyquist plots of UGA and PGA.

Figure 3A shows the CV curves of UGA and PGA in 0.5 M Na_2SO_4 electrolyte and at 20 mV/s scan rate. The CV curve of UGA is almost rectangular, the characteristic of a typical electric double-layer capacitor. The CV of PGA is similar to a rectangle, exhibiting ideal capacitance behavior. The difference in electronegativity between P and C atoms destroys the neutrality of graphene lattice and provides a more highly polarized surface, which helps to increase the capacitance of material [37]. Therefore, by comparing the CV curves of PGA and UGA, it was found that the area of PGA is larger than that of UGA, indicating that the capacitance of PGA material is much larger than that of UGA, and it has better capacitance performance.

As shown in the Nyquist plots of the UGA and PGA (Figure 3B), the resistance of PGA is very low and much smaller than UGA. This is because of the impact of high-frequency doping on electronic performance. From the high frequency to the intermediate frequency, the concave semicircle in the high-frequency region is related to the interface charge transfer resistance at the interface of electrode and electrolyte [38, 39]. The interface charge transfer resistance of PGA is smaller than that of UGA, indicating that P doping promotes charge transfer. In the low-frequency region, the PGA curve is more vertical due to the rapid transmission of ions. Because of the introduction of P into the layered graphene structure, PGA has a low charge transfer resistance and fast ion diffusion, thereby enhancing the capacitance performance.

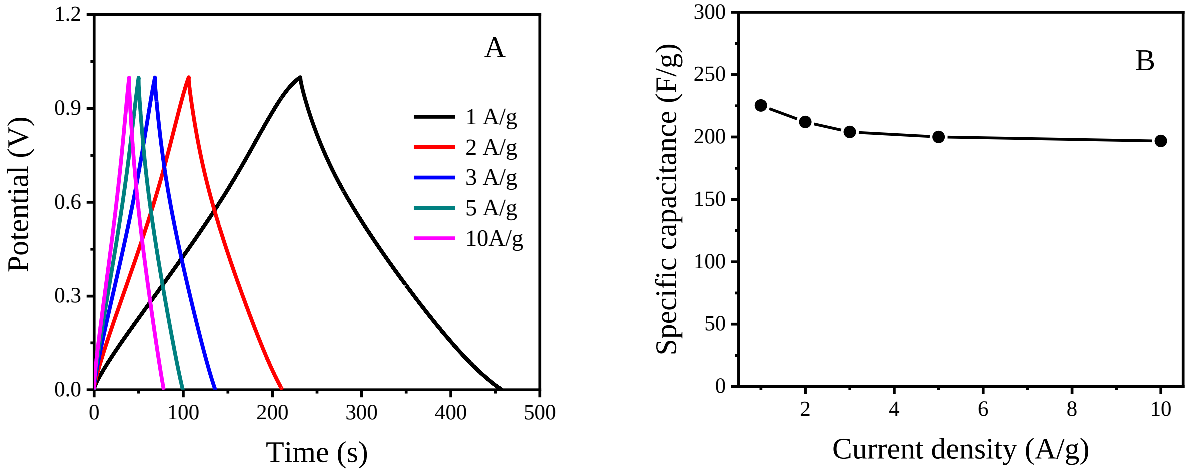

Figure 4. (A) GCD curves of PGA at various current densities from 1 to 10 A/g, (B) Cs calculated from GCD curves.

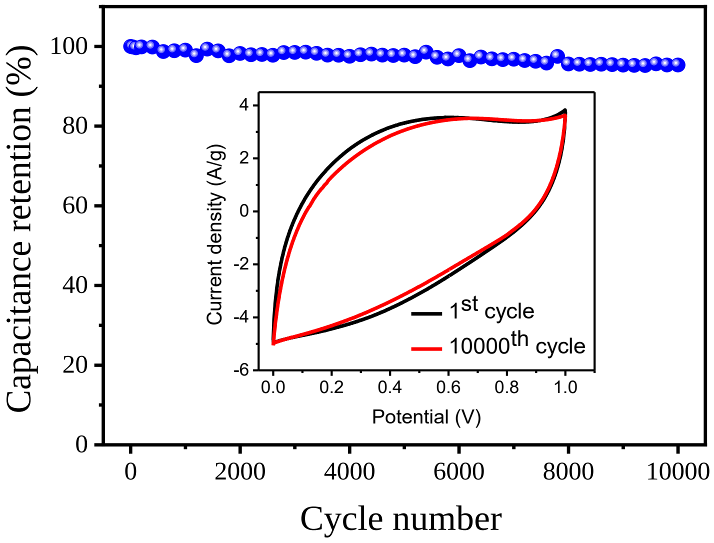

Figure 5. Cycle stability of PGA electrode at 1 A/g in 1 M Na_2SO_4 solution, (Inset: CV profile for 1st and 10,000th cycle)

Figure 4A shows the constant-current charge and discharge curves of PGA at different current densities. The constant-current charge and discharge curve of PGA is similar to an isosceles triangle, indicating that it has obvious characteristics of electric double-layer capacitance. Fig. 4B shows the Cs values obtained from galvanostatic discharge profiles. The current density increases with the decrease in Cs value, because of the decrease in ion-accessible electroactive surface. [40]. When the current density is 1, 2, 3, 5, and 10 A/g, the specific capacitance of PGA is 225.3, 212, 204, 200, and 196.8 F/g, respectively. Even if the current density is increased by 10 times, it still maintains a high specific capacitance at a high current density of 10 A/g.

Figure 5 shows the change in specific capacitance of PGA and the number of cycles when the current density is 1 A/g. After 10,000 charge-discharge cycles of PGA in Na_2SO_4 solution containing 1 mol/L electrolyte, it is reduced from 225.3 F/g to 196.8 F/g, and the capacity retention rate can reach 95%. In other words, the average capacitance loss per 100 cycles is 0.285 F/g. The inset shows a comparison of the CV curve between the 1st cycle and the 10,000th cycle. After 10,000 cycles, the CV curve hardly changes. These show that PGA materials have excellent power characteristics and chemical stability, and they are suitable as ideal capacitor electrode materials. Table 1 shows a comparison of recently reported heteroatom-doped graphene materials used for capacitor electrode. The results prove that the PGA material in this study has a better electrochemical performance compared to similar materials in the literature. This could be attributed to its hierarchical porous structure, moderate SSA and a large number of interconnected P atoms

Table 1. Partial list of reported heteroatom-doped graphene materials for supercapacitors

Electrode material	Electrolyte	Cs (F/g)
N-doped Graphene[41]	6 M KOH	109.9 (1A/g)
P-doped Graphene[42]	1 M H_2SO_4	115 (0.05A/g)
S-doped graphene[43]	6M KOH	140.8 (1A/g)
Se-doped Graphene[44]	6 M KOH	183.9 (1A/g)
N-doped Graphene[45]	6 M KOH	170.5 (0.2A/g)
PGA (this work)	6 M KOH	225.3 (1A/g)

4. CONCLUSIONS

A simple, easy-to-operate, and economical PGA was developed, where GO is the precursor and phytic acid is the predoping source of P. The layered structure of PGA electrode exhibits a large number of electrochemically active sites with a high content of heteroatoms, and P heteroatoms determine the competitive electric storage/release ability. This significantly provides, for example, a high specific capacitance of 225.3 F/g at a current density of 1 A/g. The PGA can maintain a high specific capacitance of 196.8 F/g at 10A/g and excellent capacity retention rate of 95% in 10,000 charge and discharge cycles. Therefore, PGA is feasible as an ideal electrode material for supercapacitors.

References

1. Y. Qian, F. Gao, L. Du, Y. Zhang, D. Q. Tang, D. Z. Yang, *Biosens Bioelectron.*, 74 (2015) 483.
2. J. Chang, X. Wang, J. Wang, H. Y. Li, F. Li, *Anal. Chem.*, 91 (2019) 3604.
3. T. Hou, N. N. Xu, W. X. Wang, L. Ge, F. Li, *Anal. Chem.*, 90 (2018) 9591.
4. Y. Qian, D. Tang, L. L. Du, Y. Z. Zhang, L. X. Zhang, F. L. Gao, *Biosens. Bioelectron.*, 64 (2015) 177.
5. P. P. Gai, C. C. Gu, H. Y. Li, X. Z. Sun, F. Li, *Anal. Chem.*, 89 (2017) 12293.
6. Y. Qian, T. T. Fan, P. Wang, X. Zhang, J. J. Luo, F. Y. Zhou, Y. Yao, X. J. Liao, Y. H. Li, F. L. Gao, *Sensors and Actuators B.*, 248 (2017) 187.
7. X. Z. Wang, T. Hou, T. T. Lu, F. Li, *Anal. Chem.*, 86 (2014) 9626.
8. T. Zhu, J. B. Ding, Q. Shao, Y. Qian, X. Q. Huang, *ChemCatChem.*, 11 (2019) 689.
9. M. Zhu, Q. Shao, Y. C. Pi, J. Guo, B. Huang, Y. Qian, X. Q. Huang, *Small*, 13 (2017) 1701295.
10. M. W. Zhu, Q. Shao, Y. Qian, X .Q. Huang, *Nano Energy*, 56 (2019) 330.
11. Y. Qian, C. Huang, R. Chen, S. Dai, C. Wang, *Int. J. Electrochem. Sci.,* 11 **(2016)** 7453
12. J. Huang, Y. Wang, H. C. Deng, J. Chen, J. Ding, C. Y. Wang, *Int. J. Electrochem. Sci.*, 15 (2020) 7272.
13. M. E. Kady, V. Strong, S. Dubin, R. B. Kaner, *Science*, 335 (2012) 1326.
14. X. Peng, L. Peng, C. Wu, Y. Xie, *Chem Soc Rev*, 43 (2014) 3303.
15. D. Pech, M. Brunet, H. Durou, P. Huang, V. Mochalin, Y. Gogotsi, P. L. Taberna, P. Simon, *Nat. Nanotechnol*, 5 (2010) 651.
16. X. Lang, A. Hirata, T. Fujita, M. Chen, *Nat. Nanotechnol*, 6 (2011) 232.
17. M. Kim, J. Yang, Y. Kang, S. Park, J. Han, K. Kim, K. Roh, *Colloids and Surfaces A.*, 443 (2014) 535.
18. G. Ren, Q. Chen, J. Zheng, B. Huang, Y, Qian, *J. Electroanal. Chem.*, 829 (2018) 177.
19. J. Chen, T. Zhu, X. Fu, G. Ren, C. Wang, *Int. J. Electrochem. Sci.*, 14 (2019) 7293.
20. S. Prabaharan, R. Vimala, Z. Zainal, *Journal of Power Sources*, 161 (2006) 730.
21. L. Zheng, K. S. Xia, B. Han, C. G. Zhou, Q. Gao, H. Q. Wang, S. Pu, J. P. Wu, *ACS Appl. Nano Mater.*, 1 (2018) 6742.
22. S. B. Ye, J. C. Feng, P. Y. Wu, *ACS Appl. Mater. Interfaces*, 15 (2013) 7122.
23. S. Nardecchia, D. Carriazo, M. L. Ferrer, M. C. Gutiérrez, F. del Monte, *Chem. Soc. Rev.*, 42 (2013) 794.
24. R. Dubey, V. Guruviah, *Ionics*, 25 (2019) 1419.
25. W. X. Song, J. Lischner, V. G. Rocha, H. Qin, J. H. Qi, J. H. L. Hadden, C. Mattevi, F. Xie, D. J. Riley, *ACS Energy Lett.*, 2 (2017) 1144.
26. J. P. Paraknowitsch, A. Thomas, *Energ. Environ. Sci.*, 6 (2013) 2839.
27. Z. Y. Sui, Y. N. Meng, P. W. Xiao, Z. Q. Zhao, Z. X. Wei, B. H. Han, *ACS Appl. Mater. Interfaces*, 7 (2015) 1431.
28. N. Parveen, M. O. Ansari, S. A. Ansari, M. H. Cho, *J. Mater. Chem. A*, 4 (2016) 233.
29. H. Deng, M. Zhu, T. Jin, C. Cheng, J. Zheng, Y. Qian, *Int. J. Electrochem. Sci.*, 15 (2020) 16.
30. M. Enterría, M. F. R. Pereira, J. I. Martins, J. L. Figueiredo, *Carbon*, 95 (2015) 72.
31. T. Jin, J. Chen, C. Wang, Y. Qian, L. Lu, *J. Mater. Sci.*, 55 (2020) 12103-12113.
32. X. Zhang, Z. Lu, Z. Fu, Y. Tang, D. Ma, Z. Yang, *J. Power Sources*, 276 (2015) 222.
33. W. S. Hummers, R. E. Offeman, *J. Am. Chem. Soc.*, 80 (1958) 1339.
34. Y. Qian, F. Ye, J. Xu, *Int. J. Electrochem. Sci.*, 7 (2012) 10063.
35. X. Yu, Y. B. Kang, H. S. Park, *Carbon*, 101 (2016) 49-56.
36. D. H. Jurcakova, A. M. Puziy, O. I. Poddubnaya, F. S. García, J. M. D. Tascón, G. Q. Lu, *J. Am. Chem. Soc.*, 131 (2009) 5026.
37. D. Y. Zhang, M. Han, Y. B. Li, L. Y. Lei, Y. H. Shang, K. J. Wang, Y. Wang, Z. K. Zhang, X. D. Zhang, H. X. Feng, *Electrochimica Acta*, 222 (2016) 141.
38. B. G. Choi, J. Hong, W. H. Hong, P. T. Hammond, H. Park, *ACS Nano*, 5 (2011) 7205.

39. J. P. Meyers, M. Doyle, R. M. Darling, J. Newman, *J. Electrochem. Soc.*, 147 (2000) 2930.
40. U. B. Nasini, V. G. Bairi, S. K. Ramasahayam, S. E. Bourdo, T. Viswanathan, A. U. Shaikh, *J. Power Sources*, 250 (2014) 257.
41. B. Jiang, C. Tian, L. Wang, L. Sun, C. Chen, X. Nong, Y. Qiao, H. Fu *Appl. Surf. Sci.*, 258 (2012) 3438.
42. Y. Wen, B. Wang, C. Huang, L. Wang, D. Hulicova-Jurcakova, *Chem. – A Eur. J.*, 21 (2015) 80.
43. X. Yu, H.S. Park, *Carbon*, 77 (2014) 59.
44. J. Chen, C. Lin, M. Zhang, T. X. Jin, Y. Qian, *ChemElectroChem*, 7 (2020) 3311.
45. L.B. Xing, S.F. Hou, J. Zhou, J.L. Zhang, W. Si, Y. Dong, S. Zhuo, *J. Solid State Chem.*, 230 (2015) 224.